Sonochemistry

DOI: 10.1002/anie.201005533

Efficient Sonochemistry through Microbubbles Generated with Micromachined Surfaces**

David Fernandez Rivas, Andrea Prosperetti, Aaldert G. Zijlstra, Detlef Lohse, and Han J. G. E. Gardeniers*

The phenomenon of cavitation, that is, the growth and implosion of gas/vapor bubbles in a liquid, is a process that can locally generate extreme temperatures of several thousand Kelvin[1] and, for this reason, is exploited in sonochemistry to enhance chemical conversion. This feature opens the perspective of high temperature, high-pressure, large-scale systems and therefore holds the promise of constituting a "green chemistry" with a multitude of possible applications in water treatment,[2] material synthesis, the food industry[3] and others. The "ideal" sonochemical reactor from a theoretical point of view is a single bubble trapped in an acoustically driven flask, such as in single-bubble sonoluminescence.[4] There the bubble collapses periodically and in a reproducible way, as the collapse does not disintegrate the bubble. Reactants are sucked into the bubble at expansion and reaction products leave the bubble at collapse; the typical temperatures achieved are around 15000 K.[5,6] Another advantage is that thanks to these ideal conditions, the problem is accessible to a thorough theoretical treatment whose results are in good agreement with the experimental findings.[4,5] The downside is that the absolute chemical yields are only tiny, as the ambient size of such bubbles is only in the micrometer regime. For applications, typical sonochemical reactors, such as ultrasonic baths or vessels with ultrasound (US) horns attached to their walls, are considerably larger than the active region in which cavitation occurs, which is defined by the US field that the transducer generates in the reactor. The difficulty of matching the US field with the reactor dimensions so that the complete volume of reactant can be stimulated adds to the low efficiency of most sonochemical processes. Attempts aimed at optimizing the configuration have mostly had limited success.[7–10]

Herein we present a new approach to address this problem based on the premise that significant gain in efficiency may be obtained if the location of the nucleation of bubbles, which subsequently will cavitate due to ultrasound, can be accurately controlled. Achieving this objective will give us control over the spatial distribution of cavitation events, and therewith also over the actual volume of liquid that can be exposed to sonochemical effects.

The nucleation and formation of bubbles as a result of ultrasound is mostly heterogeneous, that is, it relies on pockets of gas trapped and stabilized inside randomly existing crevices in container walls or particles suspended in the bulk fluid, rendering it extremely difficult to control and predict. The theory developed for bubble nucleation from crevices[11,12] leads the way to control nucleation. As shown in recent work,[12–15] stable and monodisperse cavitation nuclei can be formed by trapping gas in pits micromachined on a silicon surface. We use such pits, which serve as artificial crevices for bubble nucleation, to achieve higher sonochemical yields at ultrasound powers that would otherwise not produce a significant chemical effect.

The micromachined silicon substrates contained three different spatial configurations, in each case with cylindrical pits of 30 μm diameter, depth of 10 μm, and interpit distance of 1000 μm. The silicon chips were placed at the bottom of a glass container with a volume of 300 μL in which we investigated the homolytic cleavage of H_2O by sonolysis at a US frequency of 200 kHz generated by an ultrasonic transducer attached to the bottom of the chip. Three different power settings were used: low (0.074 W), medium (0.182 W), and high (0.629 W). The acoustic pressures related to these power settings were calculated to be 165, 225, and 350 kPa. At low power, it was observed that a continuous stream of microbubbles is generated from the pits at the silicon surface. With more than one pit, above a certain acoustic amplitude of around 350 kPa, the bubbles are observed to travel toward a position at the center of the pit arrangement (Figure 1).

The "mother bubble" in the pit ejects streams of microbubbles, which resemble previously reported streamers.[16,17] The observed trajectories in Figure 1 are the result of the complex interplay of primary and secondary Bjerknes forces and microstreaming. For a single pit, at low and medium US powers, the microbubbles are ejected along the symmetry axis of the oscillating mother bubble and follow an ascending trajectory until they dissolve. For low power, the situation is similar for the configurations with two and three pits. With increasing power, a drastic transition in the bubble flow pattern is observed. Beyond the transition the microbubbles move away from the symmetry axis of their respective pits

[*] MSc. D. Fernandez Rivas, Prof. Dr. H. J. G. E. Gardeniers
Mesoscale Chemical Systems Group
MESA+ Research Institute, University of Twente
ME147, PO Box 217, 7500AE Enschede (The Netherlands)
Prof. Dr. A. Prosperetti
Department of Mechanical Engineering
The Johns Hopkins University, Baltimore (USA)
Prof. Dr. A. Prosperetti, MSc. A. G. Zijlstra, Prof. Dr. D. Lohse
Physics of Fluids Group
Department of Applied Physics, Faculty of Science
University of Twente, Enschede (The Netherlands)

[**] This research was supported by the Technology Foundation STW, Applied Science Division of NOW and the Technology Programme of the Ministry of Economic Affairs, The Netherlands.

Supporting information for this article is available on the WWW under http://dx.doi.org/10.1002/anie.201005533.

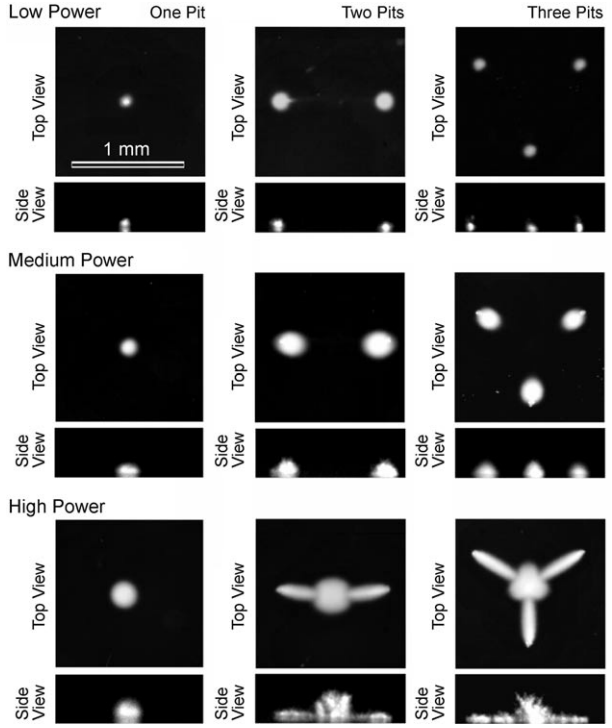

Figure 1. Top and side views of the bubble structures generated from the micropits for different configurations (one, two, and three pits) and for increasing power levels. Low power corresponds to 0.074 W and 165 kPa, medium power to 0.182 W and 225 kPa, and high power to 0.629 W and 350 kPa.

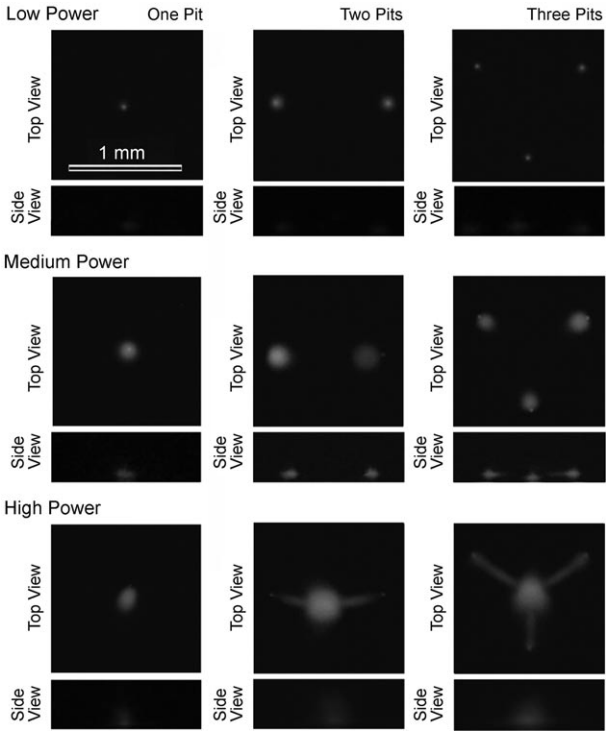

Figure 2. Luminol luminescence in dark room conditions: Top and side view of the bubble structures generated from the micropits for different configurations (one, two, and three pits) and for increasing power levels. See Figure 1.

and towards one another (see middle row in Figure 1). The microbubbles then form a dense bubble cloud traveling towards the midpoint of the two or three-pit arrangement (see Movie in the Supporting Information). For the three-pit configuration, the microstreamers point to the center of the triangular array and form a triangular cloud of bubbles, as seen in the top view.

These experiments were repeated with an aqueous solution of luminol (3-aminophthalhydrazide). Luminol is a well-established indicator for the visualization of active sonochemical regions, because it reacts with $OH^{\bullet}$ radicals to give luminescence with an intensity proportional to the amount of radicals produced.[18] Figure 2 shows the resulting images. A detailed comparison of the features in Figure 2 with those in Figure 1 reveals a perfect match.

For a quantitative measure of radical formation, we used terephthalic acid, which is a very efficient $OH^{\bullet}$ scavenger leading to the formation of hydroxyterephthalic acid (HTA). The fluorescence intensity emission of HTA at $\lambda = 429$ nm allows us to calculate the amount of radicals generated by US-induced microbubble cavitation. Similar experiments with a silicon chip with no pits showed no significant evidence of a US effect. The radical generation rates resulting from off-line fluorescence measurements are shown in Figure 3.

The data show that the presence of pits gives a significant enhancement of the radical formation rate. The rate is stable over time and is an increasing power of the US field, as expected. Radical formation increases with the number of pits, but the slope of the lines decreases as more pits are

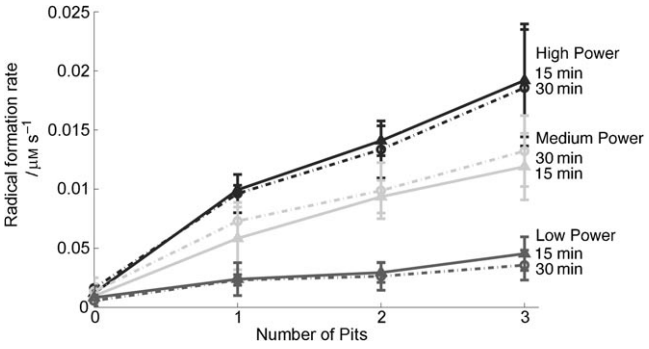

Figure 3. Radical formation rate versus number of pits (concentration increase per second). Low power = 0.074 W, medium power = 0.182 W, and high power = 0.629 W. The bars show the range of the experimental data.

added, presumably because of the onset of interactions with the bubble plumes generated by the other pits. At high power, the bubble pattern changes dramatically (Figures 1 and 2) and is expected to lead to a different radical generation distribution over the reactor volume. The quantitative interpretation of these data is complex. Generally speaking, smaller bubbles are stiffer because of a surface tension contribution and may not grow as large during expansion, leading to weaker compression and lower maximum temperatures. Large bubbles, in contrast, may not collapse spherically, especially when close to a solid surface, which would also limit their maximum compression. It is not clear, however, to what extent these general trends are relevant in the experimental situation of present concern.

The most important parameter for the evaluation of our results and comparison with the work of others is the energy efficiency defined in Equation (1), where dN_{rad}/dt is the radical formation rate in moles per second, ΔH is the energy required for the formation of OH· radicals, which is equal to the enthalpy of formation associated with Equation (2).

$$X_{US} = \frac{\Delta H dN_{rad}/dt}{P_{US}} \quad (1)$$

$$H_2O \rightleftharpoons OH + H \quad (2)$$

This enthalpy has a value of 5.1 eV per molecule.[19] P_{US} is the electric power absorbed by the transducer, which can be obtained from the measured voltage, current, and their phase difference. The efficiency as defined in Equation (1) is shown in Table 1 for each of the configurations studied.

From the values in Table 1, we can draw the following conclusions: 1) Comparing the efficiency values of the chips with one or several pits with those of the chip with no pits, there is an efficiency increase by an order of magnitude, which demonstrates that the pits on the reactor wall give a considerable enhancement. 2) The efficiency obtained even with such a low number of pits is close to the highest efficiencies reported with conventional sonochemical reactors.[20–27] A detailed comparison is hardly possible because of the use of different frequencies, chemical dosimeters, and other physical parameters.

From the values of Table 1, it can be seen that the most efficient setting is medium power in all pit configurations. Several factors may explain this observation. At high power, the microbubble collapse is more catastrophic, which results in a smaller compression and heating of the gas. In the case of two- and three-pit configuration, the microbubbles stay longer in the most active zone close to the substrate while traveling parallel to the surface; however, the collapse of microbubbles close to the surface is highly nonspherical, again reducing the maximum compression and heating of the gas. The microbubbles in the dense cloud at the midpoint may also have a weaker collapse because of shielding by the outer microbubbles. It has to be stressed that our results were obtained with only a very small active region. With state-of-the-art microfabrication procedures, it is straightforward to increase the number of pits, as shown in the Supporting Information. On the basis of our results in Table 1 and Figure 3, increasing the number of pits should give an increase in energy efficiency by a factor of 100 or more. This estimate is based on linear extrapolation of the one-, two-, and three-pit configurations at medium power settings.

Table 1: Efficiency [$\times 10^6$] as defined in Equation (1) for homolytic cleavage of H_2O by sonolysis.

	Number of pits			
	3 pits	2 pits	1 pit	0 pits
High power (0.629 W)				
15 min	4.5	3.3	2.3	0.3
30 min	4.4	3.1	2.3	0.4
Medium power (0.182 W)				
15 min	9.7	7.6	4.7	0.8
30 min	11	8.0	5.9	0.1
Low power (0.074 W)				
15 min	9.1	5.9	4.8	1.6
30 min	7.1	5.2	4.6	1.1

Our results indicate that the introduction of micromachined pits on the surface of a reactor wall attached to an ultrasound transducer can boost sonochemical efficiency. The underlying mechanism is the production of microbubble streamers from the stable gas pockets that form in these pits, and the subsequent cavitation of these microbubbles.

Received: September 3, 2010
Published online: November 9, 2010

Keywords: microreactors · radicals · sonochemistry · ultrasound

[1] K. S. Suslick, D. J. Flannigan, *Annu. Rev. Phys. Chem.* **2008**, *59*, 659–683.
[2] P. R. Gogate, *J. Environ. Manage.* **2007**, *85*, 801–815.
[3] M. Ashokkumar, D. Sunartio, S. Kentish, R. Mawson, L. Simons, K. Vilkhu, C. Versteeg, *Innovative Food Sci. Emerging Technol.* **2008**, *9*, 155–160.
[4] M. P. Brenner, S. Hilgenfeldt, D. Lohse, *Rev. Mod. Phys.* **2002**, *74*, 425–484.
[5] R. Toegel, D. Lohse, *J. Chem. Phys.* **2003**, *118*, 1863.
[6] D. J. Flannigan, K. S. Suslick, *Nature* **2005**, *434*, 52–55.
[7] K. Yasuda, T. Torii, K. Yasui, Y. Iida, T. Tuziuti, M. Nakamura, Y. Asakura, *Ultrason. Sonochem.* **2007**, *14*, 699–704.
[8] Z. Xu, C. Y. Ma, J. Y. Xu, X. J. Liu, *Ultrason. Sonochem.* **2009**, *16*, 475–480.
[9] S. Koda, K. Tanaka, H. Sakamoto, T. Matsuoka, H. Nomura, *J. Phys. Chem. A* **2004**, *108*, 11609–11612.
[10] T. Tuziuti, K. Yasui, T. Kozuka, A. Towata, Y. Iida, *J. Phys. Chem. A* **2006**, *110*, 10720–10724.
[11] A. A. Atchley, A. Prosperetti, *J. Acoust. Soc. Am.* **1989**, *86*, 1065–1084.
[12] B. M. Borkent, S. Gekle, A. Prosperetti, D. Lohse, *Phys. Fluids* **2009**, *21*, 102003.
[13] N. Bremond, M. Arora, C. D. Ohl, D. Lohse, *Phys. Rev. Lett.* **2006**, *96*, 224501.
[14] N. Bremond, M. Arora, S. M. Dammer, D. Lohse, *Phys. Fluids* **2006**, *18*, 0.
[15] P. Marmottant, J. P. Raven, H. Gardeniers, J. G. Bomer, S. Hilgenfeldt, *J. Fluid Mech.* **2006**, *568*, 109–118.
[16] T. G. Leighton, *Ultrason. Sonochem.* **1995**, *2*, S123-S136.
[17] E. A. Neppiras, *Phys. Rep.* **1980**, *61*, 159–251.
[18] A. Henglein, R. Ulrich, J. Lilie, *J. Am. Chem. Soc.* **1989**, *111*, 1974–1979.
[19] R. Toegel, S. Hilgenfeldt, D. Lohse, *Phys. Rev. Lett.* **2002**, *88*, 034301.
[20] Y. T. Didenko, K. S. Suslick, *Nature* **2002**, *418*, 394–397.
[21] M. W. A. Kuijpers, M. F. Kemmere, J. T. F. Keurentjes, *Ultrasonics* **2002**, *40*, 675–678.
[22] S. de La Rochebrochard d'Auzay, J.-F. Blais, E. Naffrechoux, *Ultrason. Sonochem.* **2010**, *17*, 547–554.
[23] V. S. Sutkar, P. R. Gogate, *Chem. Eng. J.* **2009**, *155*, 26–36.
[24] L. Hallez, F. Touyeras, J. Y. Hihn, J. Klima, J. L. Guey, M. Spajer, Y. Bailly, *Ultrasonics* **2010**, *50*, 310–317.
[25] G. Mark, A. Tauber, L. A. Rudiger, H. P. Schuchmann, D. Schulz, A. Mues, C. von Sonntag, *Ultrason. Sonochem.* **1998**, *5*, 41–52.
[26] Y. Iida, K. Yasui, T. Tuziuti, M. Sivakumar, *Microchem. J.* **2005**, *80*, 159–164.
[27] A. Mandroyan, R. Viennet, Y. Bailly, M. L. Doche, J. Y. Hihn, *Ultrason. Sonochem.* **2009**, *16*, 88–96.

